Near-ambient X-ray photoemission spectroscopy and kinetic approach to the mechanism of carbon monoxide oxidation over lanthanum substituted cobaltites

J.L. Hueso[a, b] D. Martínez-Martínez[a], A. Caballero[a, b], A.R. González-Elipe[a, b], B.S. Mun[c] and M. Salmerón[d]

[a]Instituto de Ciencia de Materiales de Sevilla (CSIC-Universidad de Sevilla), Avda. Américo Vespucio 49, 41092 Seville, Spain

[b]Departamento de Química Inorgánica, Universidad de Sevilla, C/Profesor González 1, 41071 Seville, Spain

[c]Advanced Light Source, Lawrence Berkeley National Laboratory, Berkeley, CA, USA

[d]Materials Science Division, Lawrence Berkeley Laboratory, USA

Abstract

We have studied the oxidation of carbon monoxide over a lanthanum substituted perovskite ($La_{0.5}Sr_{0.5}CoO_{3-d}$) catalyst prepared by spray pyrolysis. Under the assumption of a first-order kinetics mechanism for CO, it has been found that the activation energy barrier of the reaction changes from ~80 to ~40 kJ mol^{-1} at a threshold temperature of ca. 320 °C. In situ XPS near-ambient pressure (~0.2 torr) shows that the gas phase oxygen concentration over the sample decreases sharply at ca. 300 °C. These two observations suggest that the oxidation of CO undergoes a change of mechanism at temperatures higher than 300 °C.

Keywords: Near-ambient XPS; CO oxidation; Perovskites

Article Outline

1. Introduction

Metal oxides with perovskite structure of type ABO_3, where A is a rare-earth element and B is a transition metal, have been extensively studied as alternatives to noble metal catalysts for automotive exhaust emissions [1]. The crystalline structure and the partial substitution of some of their cations by other elements with a different oxidation state confer to these compounds very interesting properties [2] and [3] and an enhanced activity for the oxidation of (unburned) hydrocarbons [4], [5] and [6], soot particles [7] and [8] or volatile organic compounds (VOCs) [9], [10] and [11]. The oxidation of carbon monoxide has been also extensively studied not only as a model gas to prove the adsorption sites over the perovskites [12], [13] and [14], but also because of its environmental impact as one of the most hazardous pollutants produced by mobile sources [15] and [16].

Recently, we have demonstrated that the oxidation of carbon particles towards CO_2 is enhanced in the presence of cobaltites [8]. We have also shown that perovskite catalysts are very efficient for the oxidation of CO at low temperatures in a plasma-catalyst device [17] and [18]. Although the reaction mechanism of carbon monoxide over perovskites has been the subject of numerous studies during the last years, there are still many open questions requiring further considerations. Voorhoeve et al. suggested the existence of different reaction processes depending on the temperature range of reaction [1]. Tascón and co-workers analyzed the CO adsorption over $LaCoO_3$ and found that the formation of carbonate intermediates onto the catalyst surface was limited by physisorbed O_2 species occupying the same active sites required for CO adsorption [12], [13] and [14]. Viswanathan and George, based on preliminary studies of Nakamura et al. suggested that the formation of oxygen vacancies and the desorption of O_2 species play an important role in the oxidation of CO [19], [20] and [21]. This previous works agree with the formation of surface vacancies and on the adsorption of O_2 as crucial steps in the oxidation of CO. However, they disagree in the assignment of the active and adsorption sites for carbon monoxide and oxygen.

In the present work, we have studied the oxidation of carbon monoxide over a lanthanum substituted cobaltite with $La_{0.5}Sr_{0.5}CoO_{3-d}$ structure prepared by a spray pyrolysis method. Catalytic measurements, basic kinetics fittings and especially near-ambient X-ray photoemission spectroscopy (XPS) experiments have shed light over the reaction mechanism, the activation energy (E_a) values and the change of the chemical nature of the oxygen species adsorbed onto the surface of the perovskite.

2. Experimental

2.1. Catalyst preparation and characterization

A $La_{0.5}Sr_{0.5}CoO_{3-d}$ perovskite catalyst under study was synthesized by a spray pyrolysis method [8] and [22] that consists of the uniform nebulisation of nitrate solutions containing $La(NO_3)_3{\cdot}6H_2O$ (99.99%, Aldrich), $Co(NO_3)_2{\cdot}6H_2O$ (>98%, Fluka) and $Sr(NO_3)_2$ (>99%, Fluka) prepared as a 0.1 M liquid solution of precursors. Two online furnaces at 250 and 600 °C, respectively evaporate the solvent (distilled water) with the dissolved nitrates and produce an initially amorphous perovskite powder. The material is collected on a porous frit of quartz located in the outlet of the heating system. Subsequently, the amorphous powders were annealed at 600 °C for 4 h, thus obtaining a crystalline $La_{0.5}Sr_{0.5}CoO_{3-d}$ perovskite structure with rhombohedral symmetry as evidenced by X-ray diffraction (*d* represents the oxygen deficiency of the perovskite) [8] and [17]. This preparation method renders the formation of pseudo-spherical particles ranging between two microns and 45–60 nm nanocrystalline domains as determined from Scherrer calculations.

2.2. Near-ambient XPS measurements

X-ray photoemission experiments have been carried out under near-ambient pressure conditions in beamline 9.3.2. of the Advanced Light Source (ALS) at the Lawrence Berkeley Laboratory [23] and [24]. Initially, perovskites powders were pressed into pellets. An annealing pretreatment up to 550 °C in UHV conditions was initially carried out to remove adventitious carbon contamination from the sample. No significant charging effects and shifts in the photoemission peak positions were observed. Therefore, all the spectra shown in the work were plotted as initially collected. The surface oxygen associated to the perovskite lattice was taken as a reference appearing at 529.5 eV (1 eV shifted respect to its normal value of 528.5 eV) [3] and [8]. The perovskite was gradually heated up to 400 °C and “in situ” exposed to 0.2 torr of O_2. The near-ambient XPS instrument consists of a differentially pumped lens system that enables collection of photoelectrons from surface and gas species in close proximity to the sample. With this setup configuration the typical problems due to photoelectron scattering with gas molecules could be overcome for the spectra reported in the present work [25] and [26]. The incident photon energy was chosen at 685 eV and the estimated photon flux was 4×10^{14}–3×10^{15} photons s^{-1} cm^{-2}. Determination of O1s area peaks was carried out by the integration of curves after subtraction of Shirley background [27] and [28].

2.3. Catalytic oxidation tests of CO

Catalytic oxidation experiments of CO were carried out at atmospheric pressure in different apparatus consisting of a fixed-bed stainless steel U-shaped reactor [29]. An amount of 100 mg of perovskite powder was placed between quartz-wool stoppers near the center of the reactor. The temperature was controlled by a chromel–alumel thermocouple placed at the catalyst position. The reactor was placed vertically in the center of an electric furnace electronically controlled and provided with another thermocouple. Prior to the reaction, the catalyst was pre-oxidized in a stream of synthetic air (>99% purity) at 650 °C for 2 h. The reaction mixtures were fed through mass flow controllers from UNIT with a total flow of 100 sccm. The concentration of the reactants was 1% CO (1 sccm) and 6% O_2 (6 sccm) in volume, using He as gas balance (93 sccm) to dilute and avoid exothermal heating. A heating rate of 1 °C/min was used from room temperature up to 500 °C. To check the reproducibility of the results and the stability of the sample, the experimental data were acquired in three consecutive annealing/cooling cycles (≈18 h per cycle). A gas chromatograph provided with a Porapak packed column and a thermal conductimetry detector (TCD) was connected online to analyze the reaction products.

2.4. Kinetic calculations

Simple kinetics calculations have been carried out under the assumptions of (i) a first-order mechanism for the oxidation of carbon monoxide. This is supported by previous kinetics studies carried out by other authors [12], [13] and [14]. Tascón et al. suggested a weak CO adsorption especially after O_2 pre-oxidation treatments, thus further reinforcing the idea of first-order kinetics. In addition, zero and second-order approximations were also tested although larger discrepancies and errors above 20% were always obtained; (ii) the concentration of oxygen is largely in excess in comparison with CO, so the kinetics depends only on the concentration of CO, and (iii) the variation of the CO oxidation rate is linked to the variation of the overall rate constant which directly depends on temperature. The proposed formulation of the reaction rate permits the estimation of its activation energy and pre-exponential factors. The development and rearrangement of the basic kinetic equations employed has been included as Supplementary material. The final expression.

(1)

$$\ln\left\{\ln\left(\frac{[CO]_0}{[CO]}\right)\right\} = \ln(A^*) - \frac{E_a}{RT}$$

has enabled us to calculate the activation energy (E_a) from the slope of the representation of $\ln\left\{\ln\left(\frac{[CO]_0}{[CO]}\right)\right\}$ against $\frac{1}{T}$.

3. Results

3.1. Catalytic activity and kinetics analysis

Fig. 1a shows the percentage of CO conversion as a function of temperature. As can be seen nearly identical profiles are obtained after two cycles, while the third one seems to indicate certain degradation of the catalytic properties of the perovskite (see Table 1). Some structural changes may be occurring even though no appreciable changes were observed by XRD. According to Fig. 1 the $La_{0.5}Sr_{0.5}CoO_{3-d}$ cobaltite shows very small activity below 200 °C. When the temperature of reaction reaches ca. 250 °C there is a rapid increase in the percent of CO transformed into CO_2 passing from 20% to 90% in a temperature range of just 90 °C. Temperatures for 4%, 50% and 90% conversion have been gathered in Table 1. The practically constant values found for the two first reaction cycles prove that the sample maintains the same reactivity, but the increment of T_{90} after the third one indicates some degradation of the perovskite.

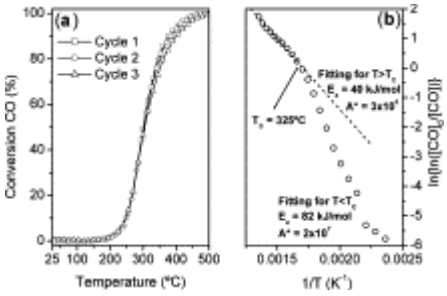

Full-size image (10K)

Fig. 1. Catalytic measurements and kinetics calculations. (a) Percentage of CO conversion as a function of temperature over the lanthanum substituted cobaltite. The experimental data have been acquired when cooling down the temperature. (b) Determination of the E_a values from expression (1) corresponding to the first oxidation cycle.

Table 1.

Selection of *n*% conversion temperatures in the reaction of CO for different consecutive cycles when cooling down the system and the corresponding calculated activation energy (E_a) and frequency factors (A).

Treatment	T_0[a]	T_{50}[b]	T_{90}[c]	E_a (1)[d]	E_a (2)[e]	$A1$[f]	$A2$[g]	T_C[h]	Error (%)
Cycle 1	220	300	375	82	40	2×10^7	4×10^3	320	4.3
Cycle 2	220	302	380	89	37	9×10^7	3×10^3	315	2.7

Treatment	T_0[a]	T_{50}[b]	T_{90}[c]	E_a (1)[d]	E_a (2)[e]	$A1$[f]	$A2$[g]	T_C[h]	Error (%)
Cycle 3	218	304	395	74	36	3×10^6	1×10^3	325	4.0

Estimated error when comparing the experimental data below 4% in all the calculations.

[a] Onset temperature for CO conversion (~3% CO conversion) expressed in °C.
[b] Temperature of 50% CO conversion expressed in °C.
[c] Temperature of 90% CO conversion expressed in °C.
[d–e] Activation energy calculated for low and high temperatures, respectively expressed in kJ mol^{-1}.
[f–g] Corresponding pre-exponential factors for the first and second region, respectively.
[h] Threshold temperature for the change of mechanism.

Fig. 1b shows that the conversion profile can be fitted according to the expression Eq. (1) presenting two different sets of apparent pre-exponential factors (A^*) and E_a values. The obtained values are summarized in Table 1 for the three oxidation cycles examined. The first reaction zone at the low temperature region presents the highest E_a values (~80 kJ mol^{-1} for all the cycles). The second region presents much lower E_a values (~40 kJ mol^{-1} for the three cycles). The change on the slope means the transition from a high to low E_a at ca. 315–325 °C. The decrease of the apparent pre-exponential factor A^* by 3–4 orders of magnitude also supports that a change of mechanism occurs around this temperature (from $A1$ to $A2$ see Table 1). In addition, the reduction of A^* in the last cycle may be indicative of a possible degradation of the catalyst (i.e. less active sites available).

3.2. Near-ambient XPS and correlation with kinetics

The assumption of a threshold temperature where a change in the reaction mechanism occurs is also supported by in situ XPS results obtained in the presence of O_2 at near-ambient pressures of ~0.2 torr. Fig. 2 presents the evolution of the O1s photoemission spectra as a function of temperature. The nature of the oxygen surface species can be ascribed to: (a) lattice oxygen of the perovskite lattice at a BE of 528.4 eV [3]; (b) hydroxides and/or carbonates species at a BE of 531 eV [30]; (c) and gas phase O_2 at 539 eV [23], [24] and [31]. In spite of the poor energy resolution it is clear that the gas peak decreases in intensity with temperature.

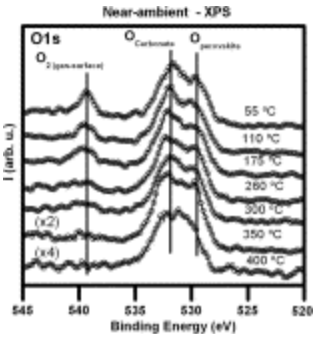

Full-size image (50K)

Fig. 2. Near-ambient pressure XPS: in situ O1s photoemission spectra of the perovskite at different temperatures in the presence of 0.2 torr of O_2 gas phase.

The peak area of this gas phase species slightly decreases in intensity up to a temperature of 300 °C and then drastically decreases to near the noise level at ca. 350 °C. The experimental evolution of the peak area ratio $O_{2gas\ phase}/O_{total}$ area with temperature has been plotted in Fig. 3a and differs from the expected evolution against temperature considering an ideal gas behaviour (dotted line in Fig. 3a). We believe that the decrease in gas phase O_2 pressure near the sample is due to the "pumping" effect of the sample that absorbs the gas to replenish the O-deficiency of the original perovskite by diffusion through oxygen vacancies [19] and [20]. It is also worth noting the sharp decrease at $T > 300$ °C coinciding with the temperature at which we have found a change in the CO oxidation kinetics. The accuracy of the kinetic model is reflected in Fig. 3b. It is shown how the experimental curves can be reproduced with a high activation energy value at low temperatures followed by a second process characterized by lower activation energy (Table 1 and Fig. 1b).

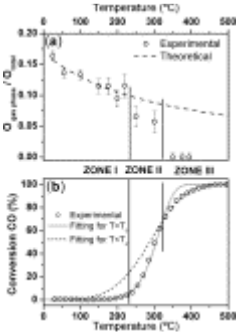

Full-size image (48K)

Fig. 3. Correlation between near-ambient XPS and CO oxidation kinetics: (a) XPS experimental evolution with temperature (open dots) and thermodynamic prediction assuming ideal gas behaviour (dashed line) of the ratio $O_{gasphase}/O_{total}$ corresponding to the peak at 539 eV. (b) Catalytic conversion of CO in the

presence of the perovskite with increasing temperatures (open dots) and comparison of the fitting curves adjusted between Eqs. (5) and (7) (see Supplementary material), using the activation energies and pre-exponential factors determined at low (grey line) and high temperature (dashed line), respectively. Vertical lines divide both plots in three temperature regions (see text for details).

The errors of these fittings have been estimated by using the following expression:

(2)

$$\text{Error} = \frac{1}{n}\sum_{T_5}^{T_{95}}\left|\frac{\%^F(T) - \%(T)}{\%(T)}\right|$$

where n is the number of experimental measurements done between T_5 and T_{95} (the temperatures of 5% and 95% conversion, respectively),$\%(T)$ represents the experimental conversion values and $\%^F(T)$ represents the conversion values from the plots obtained after fitting. The results of these calculations are below 5% for the three cycles (Table 1), which demonstrates the accuracy of the fitting and the usefulness of the mathematical model. Finally, Fig. 2 also shows a change of shape of the spectra that occurs at T = 400 °C, which might be indicative of a partial decrease in the amount of surface carbonates present on the catalyst surface [8].

4. Discussion

Fig. 3 permits to correlate the catalytic activity and the kinetic approximations carried out with the experimental evolution of the gas phase oxygen nearby the surface of the perovskite when increasing the temperature. It is important to notice the coincidence in the temperature where rapid decrease of O_2 gas phase XPS signal occurs (Fig. 3a) and the temperature where the reactivity for the CO oxidation process increases rapidly (Fig. 3b). A clear division in three different temperature regions has been established so as to explain the CO oxidation mechanism (marked by vertical lines in Fig. 3). A schematic representation is shown in Fig. 4 to illustrate the proposed reaction mechanism. In zone I (below ca. 220 °C), there is no catalytic activity, and the oxygen XPS signal evolves with temperature behaving as an ideal gas (Fig. 3 and Fig. 1). According to Tascón, in this range of temperatures the active sites for catalytic oxidation of CO are blocked by adsorbed oxygen molecules in equilibrium with the gas phase. When the temperature increases, these species can either desorb leaving additional free sites for CO adsorption or dissociate into reactive O^{2-} species.

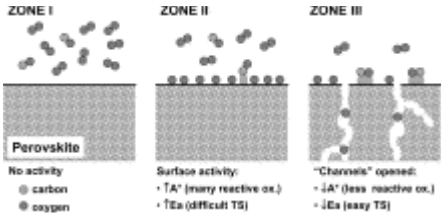

Full-size image (56K)

Fig. 4. Schematic representation of the reaction model proposed for explanation of kinetic and XPS results. Three different situations are depicted depending on the temperature.

It is at this point when rapid absorption of O_2 by the oxygen-deficient perovskite lattice takes place and where the conversion of CO increases dramatically. Therefore, we can expect a greater mobility and ionic migration of the oxygen dissociated onto the surface as temperature rises. This situation corresponds to the zone II in the reaction scheme described in Fig. 4. The onset of the reaction coincides with a first drop in the O_2 peak intensity as shown in Fig. 3. We mainly attribute this fall to the diffusion of oxygen species onto the surface of the defective perovskite occupying anionic vacancies. This fact permits the dissociation of O_2 and reaction with CO. Similar mechanisms have been proposed for gold catalysts, being the O_2 dissociation the limiting step [32]. The influence of O_2, already proposed by Tascón and co-workers can be also anticipated by our experimental results [3], [12], [13] and [14].

The boundary between zones II and III (Fig. 3 and Fig. 4) is marked by the threshold temperature (T_c = 320–325 °C) where a change of the E_a and A^* kinetics parameters is observed (Table 1) coinciding with a second drop of O_2 gas phase (above the thermodynamic predictions) detected by near-ambient XPS (Fig. 1 and Fig. 2). This threshold temperature coincides with a transition in the kinetics from high to low E_a (Table 1 and Fig. 1b). Although a compensation of kinetic parameters might explain this change, we consider that there is a direct influence of the amount of oxygen in the close vicinity of the surface of the perovskite which is intrinsically referred in the pre-exponential factor A^*. Near-ambient XPS results suggest, that since no other reactant is available, we must be attending to a process of diffusion of the oxygen species to the bulk of the perovskite lattice. We must keep in mind that the strontium substituted perovskite is oxygen defective and is provided with a high amount of vacancies [19] and [20]. This fact also explains the second deviation from thermodynamic ideal behaviour of the O_2 gas phase detected by XPS at high temperatures (Fig. 3b). Hence, it seems plausible to establish that a rate-determining step in the oxidation of CO is governed by the dissociative adsorption capacity of O_2 by the perovskite and its diffusion through oxygen vacancies (see scheme in Fig. 4).

The dissociation of O_2 limits the onset of the CO oxidation until T > 220 °C is reached. Nevertheless, the opening of ionic “channels” to facilitate the mobility of species through the bulk of the perovskite is favouring a change in the transient states of the species (see zone III in Fig. 4). According to Tascón et al. an easier adsorption and stabilization of the CO would be

enabled (Fig. 4), leading to lower values of E_a. This latter conclusion is also supported by the diminution of the pre-exponential factor A^* value (Table 1) and the release of O_2 gas phase saturation onto the surface of the catalyst. This fact also contributes to the better stabilization of the intermediate transition state (Fig. 4).

It is noteworthy that the calculated E_a are quite consistent with those previously reported by Yao [33] and slightly higher than the values proposed by Tascón et al. which might be attributed to the major dissociability of surface oxygen vacancies in our perovskite and the differences in the preparation method. Similar temperature dependences have been also observed in the oxidation of hexane over different $LaMO_3$ perovskites at 280 °C [9]. Our results are also in agreement with the suprafacial mechanism proposed by Voorhoeve et al. [1] which assumes that the mechanism of CO oxidation proceeds through the participation of adsorbed oxygen species onto the surface of the perovskite and with Nakamura et al. [19] and [20] which assumes the diffusion of oxygen as the limiting step rather than the surface reaction .

5. Conclusions

We have demonstrated the capacity of near-ambient XPS to address the influence of O_2 in the CO oxidation mechanism over a lanthanum substituted perovskite. This technique permits the direct/in situ monitorization of gas phase species in the vicinity of the surface of catalysts and has shown evidences of the active and determinant role of oxygen as controlling step of the process by surface and bulk diffusion transitions. Besides, these results have been further supported by catalytic and kinetic analyses correlating the drop of O_2 and the change of E_a values at a coinciding threshold temperature of ca. 320 °C. Therefore, we can conclude that near-ambient XPS may constitute an attractive tool for the unraveling of future reaction mechanisms at different temperatures.

Acknowledgements

This research was supported by the Spanish Ministry of Science and Education (Projects ENE2004-01660 and ENE2007-67926-C2-01). We also thank the staff of the 9.3.2 beamline at ALS facility (LNBL, Berkeley, CA) for funding and helping to accomplish the near-ambient XPS experiment. MS is funded by the Office of Basic Energy Sciences, Chemical Sciences, Geosciences and Biosciences Division under the Department of Energy Contract No. DE-AC02-05CH11231. We finally appreciate the fruitful and critical comments of the referees to improve the scientific value of the article.

References

[1] R.J.H. Voorhoeve, D.W. Johnson, J.P. Remeika and P.K. Gallagher, *Science* **195** (1977), pp. 827–833. View Record in Scopus | Cited By in Scopus (120)

[2] J.L. Hueso, J.P. Holgado, R. Pereñíguez, S. Mun, M. Salmeron, A. Caballero, Submitted for publication.

[3] L.G. Tejuca, J.L.G. Fierro and J.M.D. Tascón, *Adv. Catal.* **36** (1989), pp. 237–328. Abstract

[4] M. Alifanti, J. Kirchnerova and B. Delmon, *Appl. Catal. A-Gen.* **245** (2003), pp. 231–243. View Record in Scopus | Cited By in Scopus (40)

[5] H. Falcon, J.A. Barbero, J.A. Alonso, M.J. Martinez-Lope and J.L.G. Fierro, *Chem. Mater.* **14** (2002), pp. 2325–2333. **Full Text** via CrossRef | View Record in Scopus | Cited By in Scopus (17)

[6] S. Royer, H. Alamdari, D. Duprez and S. Kaliaguine, *Appl. Catal. B-Environ.* **58** (2005), pp. 273–288. **Article** | PDF (843 K) | View Record in Scopus | Cited By in Scopus (26)

[7] D. Fino, P. Fino, G. Saracco and V. Specchia, *Chem. Eng. Sci.* **58** (2003), pp. 951–958. **Article** | PDF (1141 K) | View Record in Scopus | Cited By in Scopus (32)

[8] J.L. Hueso, A. Caballero, M. Ocaña and A.R. González-Elipe, *J. Catal.* **257** (2008), pp. 334–344. **Article** | PDF (1381 K) | View Record in Scopus | Cited By in Scopus (3)

[9] R. Spinicci, A. Tofanari, M. Faticanti, I. Pettiti and P. Porta, *J. Mol. Catal. A-Chem.* **176** (2001), pp. 247–252. **Article** | PDF (107 K) | View Record in Scopus | Cited By in Scopus (36)

[10] V. Szabo, M. Bassir, J.E. Gallot, A.V. Van Neste and S. Kaliaguine, *Abstr. Pap. Am. Chem. Soc.* **221** (2001), p. U474.

[11] R. Pereñíguez, J.L. Hueso, J.P. Holgado, F. Gaillard, A. Caballero, Catal. Lett., in press, doi: 10.1007/s10562-009-9968-0.

[12] J.M.D. Tascón and L. González-Tejuca, *Z. Phys. Chem.-Wiesbaden* **121** (1980), pp. 63–78.

[13] J.M.D. Tascón and L. González-Tejuca, *Z. Phys. Chem.-Wiesbaden* **121** (1980), pp. 79–93.

[14] J.M.D. Tascón, J.L.G. Fierro and L.G. Tejuca, *Z. Phys. Chem.-Wiesbaden* **124** (1981), pp. 249–257.

[15] B. Viswanathan, *Catal. Rev. Sci. Eng.* **34** (1992), pp. 337–354. **Full Text** via CrossRef | View Record in Scopus | Cited By in Scopus (45)

[16] L. Simonot, F. Garin and G. Maire, *Appl. Catal. B-Environ.* **11** (1997), pp. 167–179. Abstract | PDF (722 K) | View Record in Scopus | Cited By in Scopus (56)

[17] J.L. Hueso, J. Cotrino, A. Caballero, J.P. Espinós and A.R. González-Elipe, *J. Catal.* **247** (2007), pp. 288–297. **Article** | PDF (796 K) | View Record in Scopus | Cited By in Scopus (6)

[18] J.L. Hueso, A. Caballero, J. Cotrino and A.R. González-Elipe, *Catal. Commun.* **8** (2007), pp. 1739–1742. **Article** | PDF (283 K) | View Record in Scopus | Cited By in Scopus (4)

[19] T. Nakamura, M. Misono and Y. Yoneda, *Chem. Lett.* (1981), pp. 1589–1592. **Full Text** via CrossRef

[20] T. Nakamura, M. Misono and Y. Yoneda, *Bull. Chem. Soc. Jpn.* **55** (1982), pp. 394–399. **Full Text** via CrossRef | View Record in Scopus | Cited By in Scopus (34)

[21] B. Viswanathan and S. George, *Indian J. Technol.* **23** (1985), pp. 470–472. View Record in Scopus | Cited By in Scopus (3)

[22] E. López-Navarrete, A. Caballero, V.M. Orera, F.J. Lázaro and M. Ocaña, *Acta Mater.* **51** (2003), pp. 2371–2381. **Article** | PDF (154 K) | View Record in Scopus | Cited By in Scopus (25)

[23] D.F. Ogletree, H. Bluhm, G. Lebedev, C.S. Fadley, Z. Hussain and M. Salmeron, *Rev. Sci. Instrum.* **73** (2002), pp. 3872–3877. **Full Text** via CrossRef | View Record in Scopus | Cited By in Scopus (86)

[24] Z. Hussain, W.R.A. Huff, S.A. Kellar, E.J. Moler, P.A. Heimann, W. McKinney, H.A. Padmore, C.S. Fadley and D.A. Shirley, *J. Electron Spectrosc. Relat. Phenom.* **80** (1996), pp. 401–404. Abstract | PDF (310 K) | View Record in Scopus | Cited By in Scopus (43)

[25] F.G. Requejo, E.L.D. Hebenstreit, D.F. Ogletree and M. Salmeron, *J. Catal.* **226** (2004), pp. 83–87. **Article** | PDF (265 K) | View Record in Scopus | Cited By in Scopus (11)

[26] H. Bluhm, M. Havecker, A. Knop-Gericke, E. Kleimenov, R. Schlogl, D. Teschner, V.I. Bukhtiyarov, D.F. Ogletree and M. Salmeron, *J. Phys. Chem. B* **108** (2004), pp. 14340–14347. **Full Text** via CrossRef | View Record in Scopus | Cited By in Scopus (36)

[27] QUASES, Tougaard Inc., 2007. Available in: <http://www.quases.com>.

[28] J.H. Shirley, *Phys. Rev.* **138** (1965), p. B979. **Full Text** via CrossRef | View Record in Scopus | Cited By in Scopus (590)

[29] A. Caballero, J.J. Morales, A.M. Cordón, J.P. Holgado, J.P. Espinós and A.R. González-Elipe, *J. Catal.* **235** (2005), pp. 295–301. **Article** | PDF (265 K) | View Record in Scopus | Cited By in Scopus (8)

[30] A.R. González-Elipe, J.P. Espinós, A. Fernández and G. Munuera, *Appl. Surf. Sci.* **45** (1990), pp. 103–109.

[31] K. Siegbahn, C. Nordling, G. Johansson, J. Hedman, P.F. Hedén, K. Hamrin, U. Gelius, T. Bergmark, L.O. Werme, R. Manne, Y. Baer, ESCA Applied to Free Molecules, North-Holland, Amsterdam, 1969.

[32] R. Grisel, K.J. Weststrate, A. Gluhoi and B.E. Nieuwenhuys, *Gold Bull.* **35** (2002), pp. 39–45. View Record in Scopus | Cited By in Scopus (75)

[33] Y.F.Y. Yao, *J. Catal.* **36** (1975), pp. 266–275.

Appendix A. Supplementary data

Near-ambient X-ray photoemission spectroscopy and kinetic approach to the mechanism of carbon monoxide oxidation over lanthanum substituted cobaltites

J. L. Hueso[*,a,b,d], D. Martínez-Martínez[a], A. Caballero[a,b], A. R. González-Elipe[a,b], B. S. Mun[c], M. Salmerón[c]

[a]*Instituto de Ciencia de Materiales de Sevilla (CSIC-Universidad de Sevilla). Avda. Américo Vespucio, 49. 41092. Seville (Spain).*

[b]*Departamento de Química Inorgánica, Universidad de Sevilla. C/ Profesor González, 1. 41071. Seville (Spain)*

[c]*Advanced Light Source and Molecular Foundry, Lawrence Berkeley National Laboratory, Berkeley, CA (USA)*

[d]*Present Address: Department of Chemical Engineering, University of Texas at Austin, Austin, TX 78712-1062 (USA)*

[*]To whom correspondence should be addressed: E-mail: jhueso@icmse.csic.es; Phone number: (+34) 954489500; Fax number: (+34) 954480665

(Supplementary material)

Kinetic calculations

The overall chemical reaction can be written as:

$CO + 1/2\ O_2 \rightarrow CO_2$ (1)

The equilibrium constant K ranges from ~10^{45} at 300 K to ~10^{23} at 500 K, so the reaction is assumed to be totally displaced to the right. The kinetics of the process can be described with the general equation:

$$\frac{d[CO]}{dt} = -k[CO]^n[O_2]^m \quad (2)$$

where k is the rate constant, and n and m the reaction orders for CO and O_2, respectively. Since [CO] << [O_2], and assuming a first-order mechanism for the CO (i.e. n =1) we obtain the following expression:

$$\frac{d[CO]}{dt} = -k^*[CO] \quad (3)$$

where $k^* = k[O_2]^m$. (4)

Solving the equation, we arrive to the general equation of first-order kinetics:

$$[CO] = [CO]_0 \, exp(-k^* t) \quad (5)$$

or the equivalent one:

$$k^* t = ln\left(\frac{[CO]_0}{[CO]}\right) \quad (6)$$

The variation of the concentration of CO is associated with the time of residence of CO inside the reactor. Since the gas flow is kept constant, we can also assume that the time of residence t of the reactants within the reactor remains constant. Under all these assumptions, the variation of the concentration of CO with temperature can be linked to the change of the rate constant with temperature, according to the Arrhenius equation:

$$k = A\,exp\left(-\frac{Ea}{RT}\right) \quad (7)$$

where Ea is the activation energy, A is the preexponential factor and R is the gasses'

constant. Multiplying expression (7) by the constant factor $[O_2]^m t$ and using expression (4) we can write:

$$k^* t = A^* exp\left(-\frac{Ea}{RT}\right) \quad (8)$$

being $A^* = A[O_2]^m t$.

Then, by comparing expressions (6) and (8), we obtain:

$$ln\left(\frac{[CO]_0}{[CO]}\right) = A^* exp\left(-\frac{Ea}{RT}\right) \quad (9)$$

where the dependence of [CO] with the temperature can be directly assessed.

By reordering (9):

$$ln\left\{ln\left(\frac{[CO]_0}{[CO]}\right)\right\} = ln\left(A^*\right) - \frac{Ea}{RT} \quad (10) \text{ (expression 1 in the main text)}$$

According to this expression, the Activation Energy (E_a) can be obtained from the slope of the representation of $ln\left\{ln\left(\frac{[CO]_0}{[CO]}\right)\right\}$ against $\frac{1}{T}$.